



HAL
open science

Dynamics of the Blade Channel of an Inducer under Cavitation-Induced Instabilities

Angelo Pasini, Ruzbeh Hadavandi, Dario Valentini, Giovanni Pace, Luca D'agostino

► **To cite this version:**

Angelo Pasini, Ruzbeh Hadavandi, Dario Valentini, Giovanni Pace, Luca D'agostino. Dynamics of the Blade Channel of an Inducer under Cavitation-Induced Instabilities. 17th International Symposium on Transport Phenomena and Dynamics of Rotating Machinery (ISROMAC2017), Dec 2017, Maui, United States. hal-02981026

HAL Id: hal-02981026

<https://hal.science/hal-02981026v1>

Submitted on 27 Oct 2020

HAL is a multi-disciplinary open access archive for the deposit and dissemination of scientific research documents, whether they are published or not. The documents may come from teaching and research institutions in France or abroad, or from public or private research centers.

L'archive ouverte pluridisciplinaire **HAL**, est destinée au dépôt et à la diffusion de documents scientifiques de niveau recherche, publiés ou non, émanant des établissements d'enseignement et de recherche français ou étrangers, des laboratoires publics ou privés.



Distributed under a Creative Commons Attribution 4.0 International License

Dynamics of the Blade Channel of an Inducer under Cavitation-Induced Instabilities

Angelo Pasini^{1*}, Ruzbeh Hadavandi², Dario Valentini², Giovanni Pace², Luca d'Agostino¹



ISROMAC 2017

International
Symposium on
Transport
Phenomena and
Dynamics of
Rotating Machinery

Hawaii, Maui

December 16-21
2017

Abstract

A high-head three-bladed inducer has been equipped with pressure taps along the blade channels to characterize the dynamics of the axial pump in view of a deeper insight of the cavitation-induced instabilities. The spectral analysis of the pressure signals located in both the stationary and rotating frames has allowed to characterize the nature and intensity of the principal flow instabilities detected during the experimental campaign: a sub-synchronous rotating cavitation, a cavitation surge and a high order axial oscillation. A model of the dynamics of the blade channels, that relies on experimental data and on a suitable modelling of the mean flow and cavitating volume oscillations, has been used to estimate, for all the relevant flow coefficients, the intensity of flow oscillations associated to the cavitation surge generated by the rotating cavitation.

Keywords

Cavitation — Inducer — Instability

¹Department of Civil and Industrial Engineering, University of Pisa, Pisa, Italy

²Chemical Propulsion, SITAEL S.p.A., Pisa, Italy

*Corresponding author: angelo.pasini@unipi.it

INTRODUCTION

Liquid-fed rocket engines still play a crucial role in primary space propulsion systems. In these applications propellant feed turbopumps are one of the most important components, whose design and operation are critical for the success of the mission. Modern turbopumps need to be high power density, dynamically stable machines capable of meeting the extremely demanding suction, pumping and reliability requirements of modern Space Transportation Systems.

The attainment of such high power/weight ratios is invariably obtained by running the impeller at the maximum allowable speed and lower shaft torque. Operation under cavitating conditions with lighter – but also more flexible – shafts is therefore tolerated, exposing rocket propellant feed turbopumps to the onset of dangerous cavitation-induced fluid dynamic and rotordynamic instabilities that can be easily responsible for catastrophic failures of the machine.

Cavitation represents the major source of degradation of their suction performance, efficiency, reliability, power density and useful life [1]. More importantly for space applications, cavitation can provide the necessary flow excitation and compliance for triggering dangerous fluid mechanic and/or rotordynamic instabilities of the turbopump [2, 3, 4, 5, 6, 7, 8, 9, 10, 11], or even, through the coupling with thrust generation and the structural response, of the entire space vehicle (POGO auto-oscillations, [12, 13]). The rotating cavitation in combination with the corresponding cavitation surge usually excited by the azimuthal instability are the most dangerous cavitation induced instabilities [14] for the

introduction of both unsteady rotordynamic forces and significant flow oscillations that can couple with either the rotordynamic of the impeller or the dynamics of the combustion chamber.

The present paper illustrates the results of an experimental campaign performed on a three-bladed inducer, named RAPDUD, at SITAEL S.p.A. in the Cavitating Pump Rotordynamic Test Facility (CPRTF), which is used to carry out tests on turbomachines under thermal and fluid dynamic similarity by using water at different temperatures. The dynamics of the blade channel have been experimentally assessed under typical flow regimes characterized by flow instabilities in both non-cavitating and cavitating conditions.

A special focus has been devoted to the characterization of the most dangerous cavitation-induced instabilities such as the rotating cavitation and the cavitation surge detected both at low frequencies (classical low order instabilities) and at high frequencies (high order instabilities). The experimental data have been integrated in a suitable developed analytical model of the dynamics of the blade channels.

1. EXPERIMENTAL APPARATUS AND PROCEDURE

1.1 Test Rig

The CPRTF is a versatile and easily instrumentable test rig that operates in water at temperatures up to 90 °C [15]. The facility is intended as a flexible apparatus that can readily be adapted to conduct experimental investigations on virtually any kind of fluid dynamic phenomena relevant to high performance turbopumps in a wide variety of alternative configurations (impeller with

axial, radial or mixed flow, with or without an inducer). The CPRTF has been especially designed for the analysis of unsteady flow phenomena and the measurement of fluid-induced rotordynamic forces on impellers in scaled cavitation tests under fluid dynamic and thermal cavitation similarity conditions (see Figure 1).

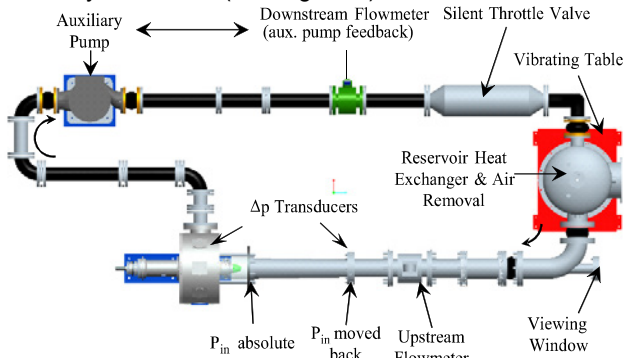


Figure 1. The Cavitating Pump Rotordynamic Test Facility

The facility has been specifically instrumented in order to characterize the pumping and suction performance of the RAPDUD inducer, as well as to characterize the typical flow instabilities generated by cavitation [16]. In particular, pressure transducers have been placed on the casing of the pump, made of Plexiglas, which allows also for optical access to the inducer flow. Eight PCB S112A22 piezoelectric pressure transducers have been flush mounted on the Plexiglas at several axial and azimuthal positions (Figure 2). At each axial station up to five transducers can be mounted with a given angular spacing, in order to cross-correlate their signals for amplitude, phase and coherence analyses. Cross-correlation of two pressure signals from different locations allows for determining the axial or azimuthal nature of each instability and, in the second case, the number of rotating cells involved.

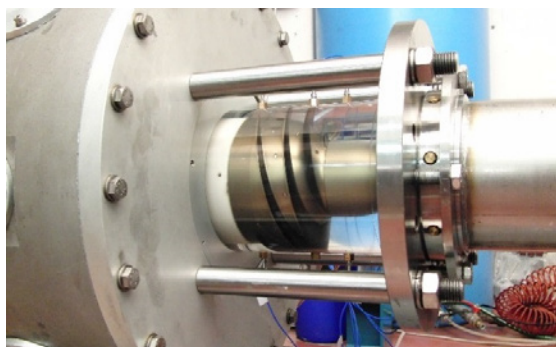


Figure 2. Test Section of the Cavitating Pump Rotordynamic Test Facility at SITAEL S.p.A.

In the present experimental campaign, additional piezoresistive Kulite XTM-190M pressure transducers have been flush mounted on the inducer hub (Figure 3). A similar approach was exploited by Fujii et al. [17], who placed pressure transducers at the trailing edge of an inducer in order to characterize the number of rotating cavitation cells.

Hence, the effects of the typical cavitation-induced instabilities, already detected in the stationary frame, have been characterized also in the rotating frame. In the present work, the results obtained for the characterization of the fluid instabilities developed along the blade channel are presented. Five different pressure taps are made available on the inducer hub along each blade channel (see Figure 4 and Table 1). In the present work, three different positions were exploited for the evaluation of the results: position PT1, PT2, and PT5.

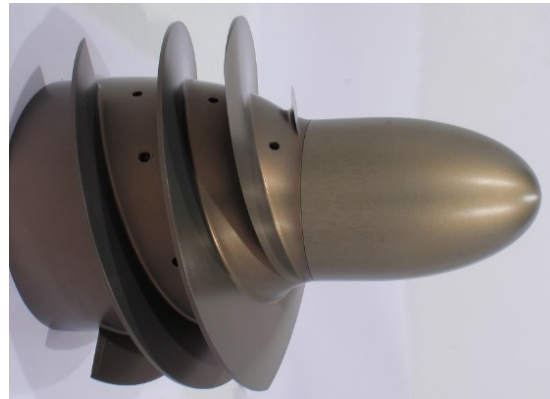


Figure 3. The RAPDUD inducer equipped with pressure taps along the blade channels

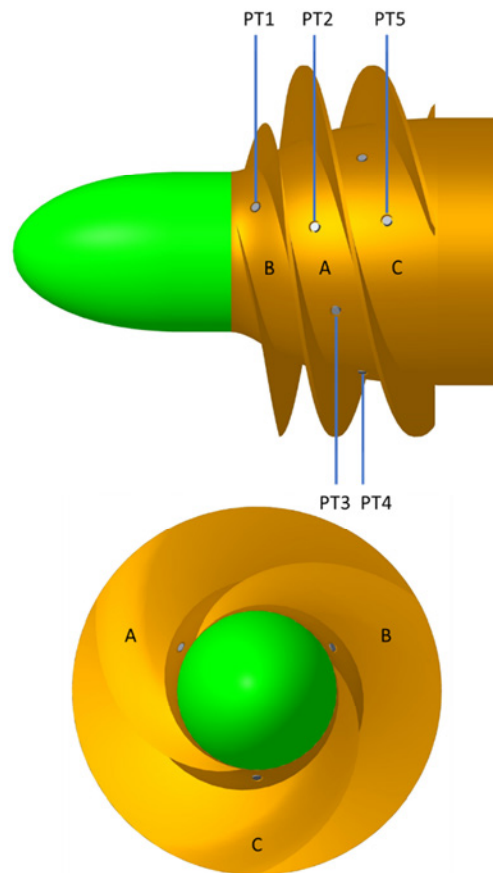


Figure 4. Pressure taps position in the blade channels

Table 1. Radial and chord-wise position of the pressure transducers (percentage with respect to the fully bladed chord length measured at the hub)

	Chord wise [%]	Radius [mm]
PT1	-22.2	38.56
PT2	26.5	51.3
PT3	41.6	53.2
PT4	58.5	55.7
PT5	72.2	57.0

The operating conditions for the Kulite transducers on the inducer hub are very critical due to the contemporary presence of cavitation bubbles which can collapse directly on the transducers membrane, and of steady centrifugal acceleration which can rise up to almost 700 g at 3000 rpm for the transducers positioned at the greatest distance from the rotational axis. For this reason, the Kulite transducers with 0÷3.5 bar of pressure range have been positioned at the inlet of the channel while 0÷7 bar pressure range have been positioned in the rest of the channel, where the stresses are considerably higher.

The main characteristics of the two types of transducers are shown in Table 2.

Table 2. Main characteristics of the Kulite XTM-190M and PCB S112A22

	Kulite	PCB Piezotronics	Unit
Model	XTM-190M	S112A22	
Technology	Piezo-resistive	Piezo-electric	
Pressure Range	0 ÷ 3.5 (A) 0 ÷ 7 (B)	0 ÷ 3.45	bar
Sensitivity	0.01	1.45	V/bar
Resolution	Infinitesimal	0.007	kPa
Temperature Range	-29 ÷ 175	-73 ÷ 135	°C
Natural Frequency	95 (A) 125 (B)	250	kHz
Error (Combined Non-Linearity, Hysteresis and Repeatability)	± 1 %	≤ 1 %	FS

In addition, the test equipment includes (see Figure 1):

- two electromagnetic flowmeters (Fisher-Rosemount, model 8732E, range: 0-100 l/s, accuracy 0.5% FS), for the measurement of the inlet and outlet flow rates;
- two absolute pressure transducers placed, respectively, 1 and 6 diameters upstream the blade leading edge (GE, model Druck PMP1400, range 0÷1 bar, accuracy 0.25% FS; GE, model UNIK5000, range 0÷2 bar, accuracy 0.1% FS) for the assessment of the inlet cavitation number;
- two differential pressure transducers to measure the pump pressure rise between inlet stations placed, respectively, 1 and 6 diameters upstream the blade

leading edge and outlet station placed about two diameters downstream the blade trailing edge (GE, model UNIK5000, range 0÷1 bar, accuracy 0.1% FS; GE, model UNIK5000, range 0÷5 bar, accuracy 0.1% FS);

- one temperature sensor PT100 (range 0÷100 °C, accuracy 0.5°C);
- a photo camera and a high speed video camera for visualization of cavitating flow around the inducer.

1.2 Test Item

The inducer tested in the present campaign is named RAPDUD. It is a three-bladed high head inducer with tapered hub and variable pitch whose main characteristics are summarized in Table 3.

The design of the inducer has been based on the mathematical model developed at ALTA S.p.A. and previously used for the design of other inducers [15, 18].

Table 3. Most relevant geometrical and operational parameters for the RAPDUD inducer

Blade number	[-]	N_{blade}	3
Tip radius	mm	r_T	81
Inlet tip blade angle	deg	γ_{Tle}	82.8
Outlet tip blade angle	deg	γ_{Tte}	79.65
Inlet hub radius (fully-developed blade)	mm	r_{Hle}	45
Outlet hub radius	mm	r_{Hte}	58.5
Axial length (fully-developed blade)	mm	c_a	69
Tip solidity	[-]	σ_T	2.28
Design flow coefficient	[-]	Φ_D	0.070
Overall Axial length	mm	L	90
Clearance	mm	cle	0.8
Mean blade height	mm	h_m	29.25

1.3 Experimental Procedure

In the cavitating experiments, the test data have been taken keeping the flow coefficient and the pump rotational speed constant while gradually reducing the inlet pressure from atmospheric conditions to the minimum allowable value at a constant rate of about 4 mbar/s.

During the data reduction, two components of the signal of the pressure transducers are identified: a quasi-static component (\bar{p}) that is weakly changing during the pressure ramp; an unsteady component (\tilde{p}) associated to the flow instabilities.

$$p = \bar{p} + \tilde{p} \cong \bar{p} + \sum_{n=0}^{N-1} \hat{p}_{\omega_n} e^{-i\omega_n t} \quad (1)$$

The unsteady component is then approximated by the discrete inverse Fourier transformation obtained by a suitable spectral analysis (see Table 4). The same approach is used to characterize the volumetric flow rate.

$$\dot{V} = \bar{V} + \tilde{V} = \bar{V} + \sum_{n=0}^{N-1} \hat{V}_{\omega_n} e^{-i\omega_n t} \quad (2)$$

Table 4. Relevant data for the spectral analysis

Spectral Analysis	
Overall Test Duration	240 s
Sample Rate	5000 Hz
Record of Samples	10000
Number of Records	4
Records Overlapping	50%
Windowing	Hann

2. DYNAMICS OF THE BLADE CHANNELS

Between two generic sections along the circuit (denoted by the subscripts u and d , respectively, for the upstream and downstream locations) and for each of the relevant harmonic oscillations, the corresponding oscillations of the pressure, of the volumetric flow rate and of the cavitating volume entrapped between the two sections are, respectively, defined as follows:

$$\tilde{p}_{u,d} = \hat{p}_{u,d} e^{-i\omega t} \quad \tilde{V}_{u,d} = \hat{V}_{u,d} e^{-i\omega t} \quad \tilde{V}_C = \hat{V}_C e^{-i\omega t} \quad (3)$$

The same oscillations can be expressed in terms of dimensionless quantities by means of a suitable definition of the unsteady static pressure coefficient and flow coefficient:

$$\hat{\psi}_{u,d} = \frac{\hat{p}_{u,d}}{\rho_L \Omega^2 r_T^2}; \quad \hat{\phi}_{u,d} = \frac{\hat{V}_{u,d}}{\pi \Omega r_T^3}; \quad \hat{\phi}_{V_C} = \frac{\hat{V}_C}{\pi \Omega r_T^3} = -i \left(\frac{\omega}{\Omega} \right) \frac{\hat{V}_C}{\pi r_T^3} \quad (4)$$

2.1 Continuity Equation

The quasi-static mass flow rate is the same in the upstream and downstream sections ($\dot{V}_u = \dot{V}_d$) because the test is performed at constant flow rate. According to the unsteady continuity equation, the perturbative terms differ between the two sections because of the oscillation of the cavitating volume:

$$\hat{\phi}_d - \hat{\phi}_u = -i\omega \frac{\hat{V}_C}{\pi \Omega r_T^3} = \hat{\phi}_{V_C} \quad (5)$$

2.2 Momentum Equation

In the quasi-static approximation (i.e. negligible inertial effects), the static head coefficient of an impeller is only a function of the flow coefficient and the cavitation number.

$$\psi = \psi(\phi, \sigma) \Rightarrow d\psi = \frac{\partial \psi}{\partial \phi} \Big|_{\sigma} d\phi + \frac{\partial \psi}{\partial \sigma} \Big|_{\phi} d\sigma \quad (6)$$

By introducing the inertance [19] of the impeller in order to take into account the inertial effects, the oscillations in the head coefficient depend on the oscillations in the mean flow coefficient and in the cavitation number according to the following equation:

$$\hat{\psi}_d - \hat{\psi}_u = 2 \frac{\partial \psi}{\partial \sigma} \Big|_{\phi} \hat{\psi}_u + \left[\frac{\partial \psi}{\partial \phi} \Big|_{\sigma} + i \frac{\omega}{\Omega} \left(\frac{\rho}{\rho_L} \right) \pi r_T \int_{x_u}^{x_d} \frac{dx}{A} \right] \hat{\phi} \quad (7)$$

The mean flow coefficient oscillation can be defined as the average oscillation between the upstream and downstream sections, while the oscillation in the cavitation number can be approximated by the oscillation in the upstream unsteady pressure coefficient as long as the pressures used to compute these dimensionless numbers differ only by an offset:

$$\hat{\phi} = \frac{1}{2} (\hat{\phi}_d + \hat{\phi}_u) \quad \hat{\sigma} \cong 2\hat{\psi}_u \quad (8)$$

2.3 Mean Flow and Cavitating Volume Oscillations

From the momentum equation, the mean flow coefficient oscillation can be obtained from the pressure oscillations measured upstream and downstream the impeller once the characteristic performance surface of the pump has been experimentally determined ($\psi = \psi(\phi, \sigma)$) and the inertance of the pump characterized.

$$\hat{\phi} = \frac{\left[\hat{\psi}_d - \left(1 + 2 \frac{\partial \psi}{\partial \sigma} \Big|_{\phi} \right) \hat{\psi}_u \right]}{\left[\frac{\partial \psi}{\partial \phi} \Big|_{\sigma} + i \frac{\omega}{\Omega} \left(\frac{\rho}{\rho_L} \right) \pi r_T \int_{x_u}^{x_d} \frac{dx}{A} \right]} \quad (9)$$

On the other side, the oscillations in the upstream and downstream sections can be computed from the continuity equations once the cavitating volume oscillations have been experimentally or theoretically assessed:

$$\begin{cases} \hat{\phi}_u = \hat{\phi} - \frac{1}{2} \hat{\phi}_{V_C} \\ \hat{\phi}_d = \hat{\phi} + \frac{1}{2} \hat{\phi}_{V_C} \end{cases} \quad (10)$$

If the cavitating volume is not significantly oscillating (i.e. negligible variation of the unsteady flow coefficient due to the increase or decrease of the cavitating volume), the flow rate oscillations are almost the same in the upstream and downstream sections and both roughly coincide with the mean flow oscillations.

On the contrary, when the cavitating volume is violently oscillating, the mean flow coefficient oscillation is negligible, and the upstream and downstream oscillations have roughly the same intensity but opposite phase.

3. RESULTS AND DISCUSSION

3.1 Cavitating Performance

Figure 5 reports the cavitating performance at 3000 rpm of the RAPDUD inducer in cold water (i.e. 20°C) for a wide range of flow coefficients (from 80% to 120% of the design condition). The reported head coefficient refers to the static head rise measured by means of the pressure taps located in the stationary frame far upstream (6 diameters) and far downstream the inducer (2 diameters).

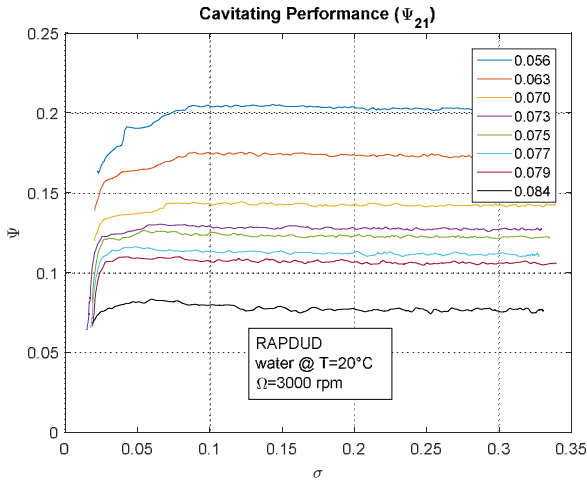


Figure 5. Cavitating performance of the RAPDUD inducer in cold water from 80% to 120% of the design flow coefficient

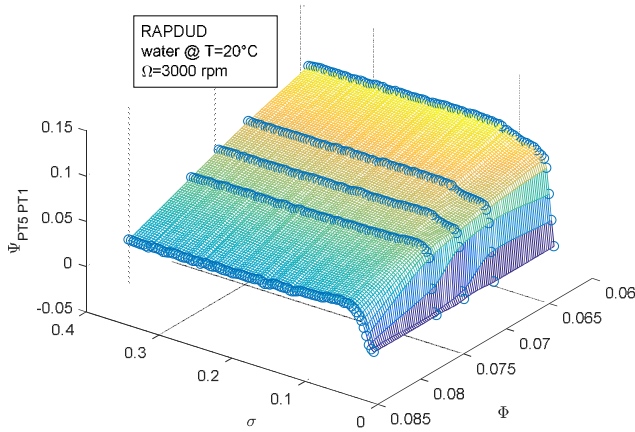


Figure 6. Head coefficient across the blade channel as a function of cavitation number and flow coefficient

The head coefficient measured by the pressure transducers located in the rotating frame along the blade channel in the first and last positions of the pressure taps (respectively PT1 and PT5) is shown in Figure 6. In this case, the experimental data are arranged in such a way that the resulting characteristic surface can be used both for assessing the cavitating performance and for estimating the gradient of the head coefficient in its main independent variables (such as the flow coefficient and the cavitation number).

Both Figure 5 and Figure 6 report an integral average value of the head coefficient obtained according to the following steps:

- the signal is numerically integrated in time and the corresponding cumulative integral is evaluated on the same samples of the original signal (5000 sps);
- the cumulative signal is then sampled at lower frequency (1 sps);
- the average value is obtained numerically as the slope of the cumulative integral signal sampled at lower frequency.

3.2 Flow Instabilities

The pressure transducers mounted in the rotating frame allow for measuring the local cavitation number along the blade channels. The first pressure tap (PT1) is located upstream of the fully-developed blade channel in the region in which the leading edge develops from the hub to the tip. While the second pressure tap (PT2) and the last one (PT5) are located, respectively, at the inlet and outlet of the channel in the fully-bladed portion of the inducer.

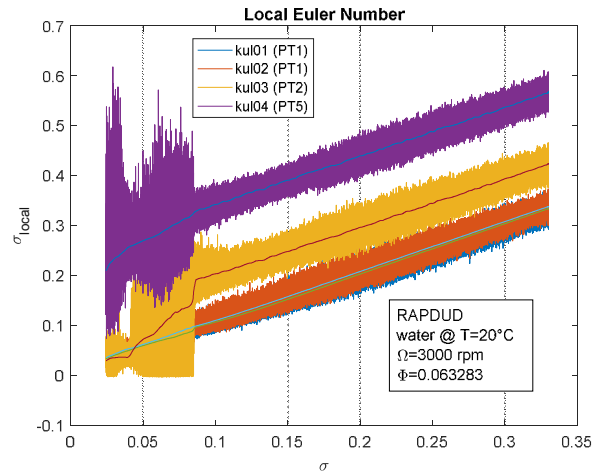


Figure 7. Local cavitation number measured through the pressure taps located along the channels during the test at 90% Φ_D

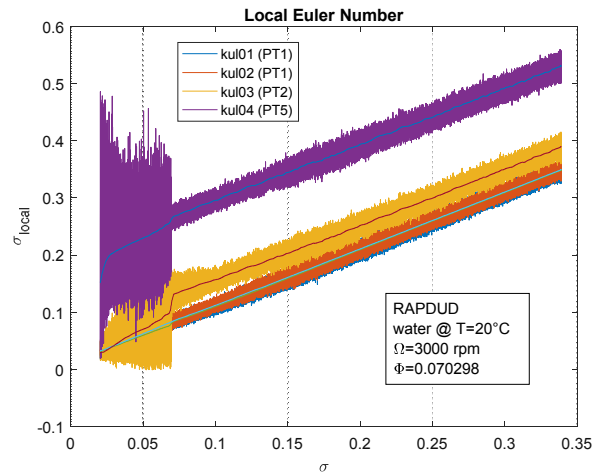


Figure 8. Local cavitation number measured through the pressure taps located along the channels during the test at 100% Φ_D

Figure 7 reports the local cavitation number measured in the rotating frame along the different pressure tap locations as a function of the cavitation number during the test performed at 90% Φ_D . A violent pressure oscillation is detected in the blade channel, especially by the pressure transducer located at the inlet of the channel (PT2), once the inlet cavitation number goes below a certain threshold value (roughly 0.08 for this flow coefficient). It is worth noticing that during this violent oscillation, the minimum

values of the local cavitation number at PT2 is roughly equal to zero and, consequently, the local pressure is close to the vapor pressure of the fluid. Therefore, the corresponding pressure transducer is experiencing a violent pressure oscillation between the completely cavitating condition (vapor pressure) and the consequently pressure peaks associated to the collapse of the cavitating region (fully wetted flow).

This happens also at higher flow coefficient conditions with typically progressively less intensity (from 90% to 105% Φ_D as reported from Figure 7 to Figure 9) until this phenomenon completely disappears at quite high flow coefficient (such as at 110% Φ_D as highlighted in Figure 10).

The nature and intensity of the cavitation induced flow instabilities have been studied through the pressure transducers located both in the stationary and rotating frames.

From the analysis of the spectra and the phases of the cross-spectra (see Figure 11 and Figure 12) of the pressure transducers located in the stationary frame at the inlet of the inducer, the violent oscillation is associated to the onset of a sub-synchronous rotating cavitation instability (RC) that eventually leads to a cavitation surge (CS) at lower frequency (equal to $\Omega - f_{RC}$). As confirmed by the cross-spectrum phases, the rotating cavitation is a one lobe sub-synchronous co-rotating instability while the cavitation surge is an axial oscillation with zero-value of the phase of the cross-spectrum for all the couples of transducers reported. The spectra of the transducers present other peaks related to the passage of the blades and its non-linear interaction with the rotating cavitation and cavitation surge instabilities. There is also an axial oscillation (AO) of the flow at relative high value of the cavitation number at a high frequency (roughly 7Ω) compatible with a high order surge instability.

The corresponding spectral analysis performed in the rotating frame for the same test at 90% Φ_D is reported in Figure 13 and Figure 14. The spectra of the pressure signals clearly highlight the same instabilities with some caveats, such as the frequency shifting for the rotating instabilities. In particular, the high order axial oscillation is detected at the same frequency, while the rotating cavitation is detected at a lower frequency (i.e. $|f_{RC} - \Omega|$) as a one lobe counter-rotating instabilities, which is highlighted by the cross-spectrum between the two pressure transducers – kul01 and kul02 - located at the first station at the same axial location, PT1. In fact, the angular space between the two transducers is equal to 120° while the phase of the cross-spectrum is roughly -120° . In the rotating frame, the cavitation surge is not clearly detectable because it has the same modulus of the frequency of the rotating cavitation (i.e. $|\Omega - f_{RC}|$).

By comparing the intensity of the pressure oscillations at the different locations along the channel (see Figure 13), the strongest oscillation associated to the rotating cavitation is detected by the pressure transducer located at the inlet of the channel (i.e. PT2).

Finally, the analysis of the cross-spectrum between kul01 and kul02 (Figure 14) allows for identifying another weak axial oscillation at a frequency equal to $N_{blade}|\Omega - f_{RC}|$ associated to the interaction of the three channel with the rotating cavitation instability [20].

As already mentioned, an increase of the flow coefficient implies a reduction in the intensity of the flow oscillation associated with the rotating cavitation that yields eventually to the vanishing of this instability as reported in Figure 10 for 110% Φ_D . This is also evident in the cavitating performance curve that presents a slightly increase of the head coefficient instead of the sharp pressure drop associated to the rotating cavitation instability (see Figure 5). The pressure oscillations still recorded at low cavitation number at the outlet of the channel (i.e. PT5) refer to an axial instability.

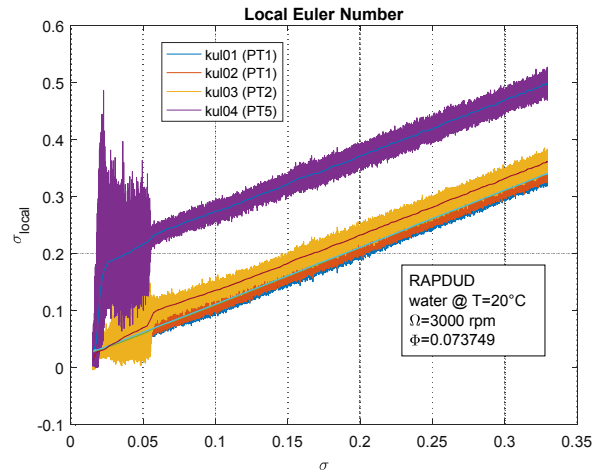


Figure 9. Local cavitation number measured through the pressure taps located along the channels during the test at 105% Φ_D

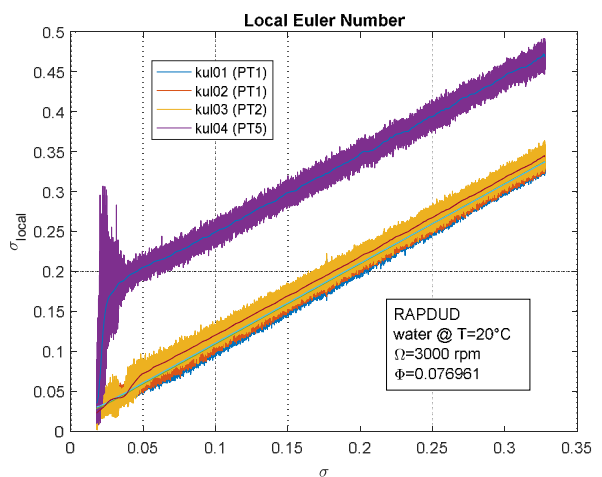


Figure 10. Local cavitation number measured through the pressure taps located along the channels during the test at 110% Φ_D

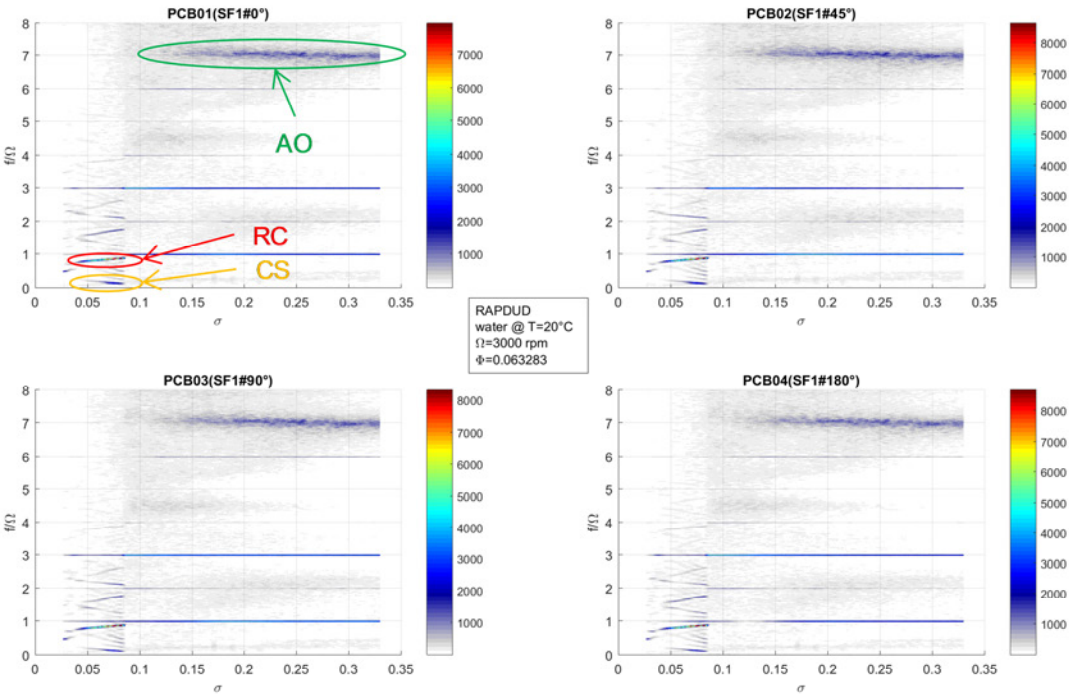


Figure 11. Spectrum of the amplitude of the harmonic pressure oscillations ($|\hat{p}|$) measured by the pressure transducers located in the stationary frame at the inlet section during the test at 90% Φ_D (measured in Pa)

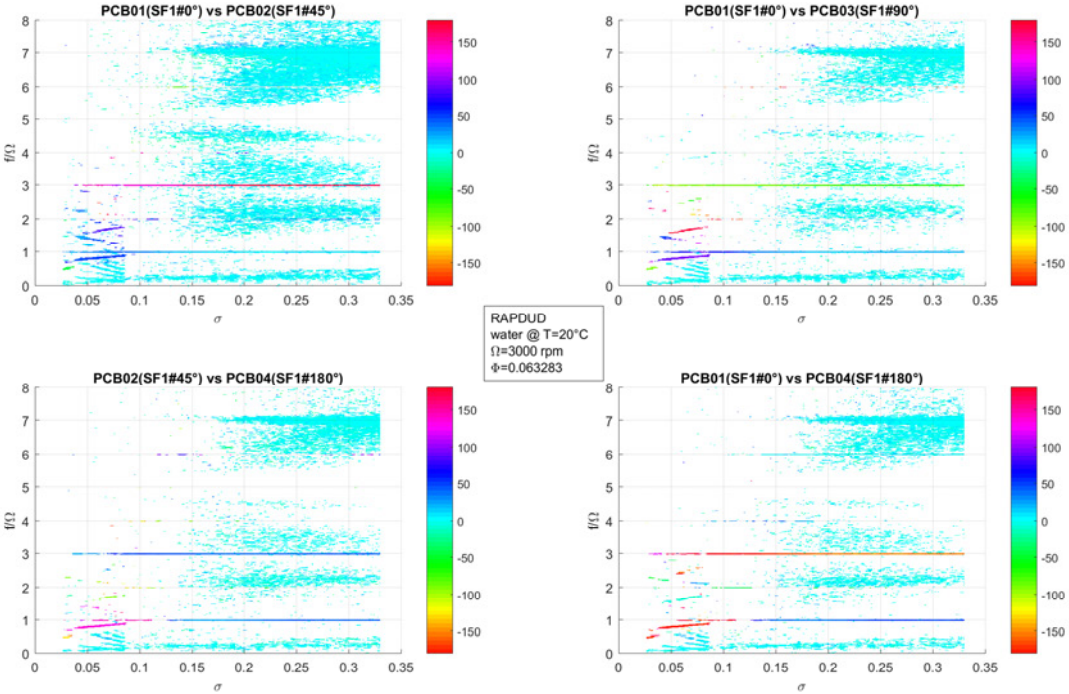


Figure 12. Phases of the cross-spectra of the pressure transducers located in the stationary frame at the inlet section during the test at 90% Φ_D (measured in degrees)

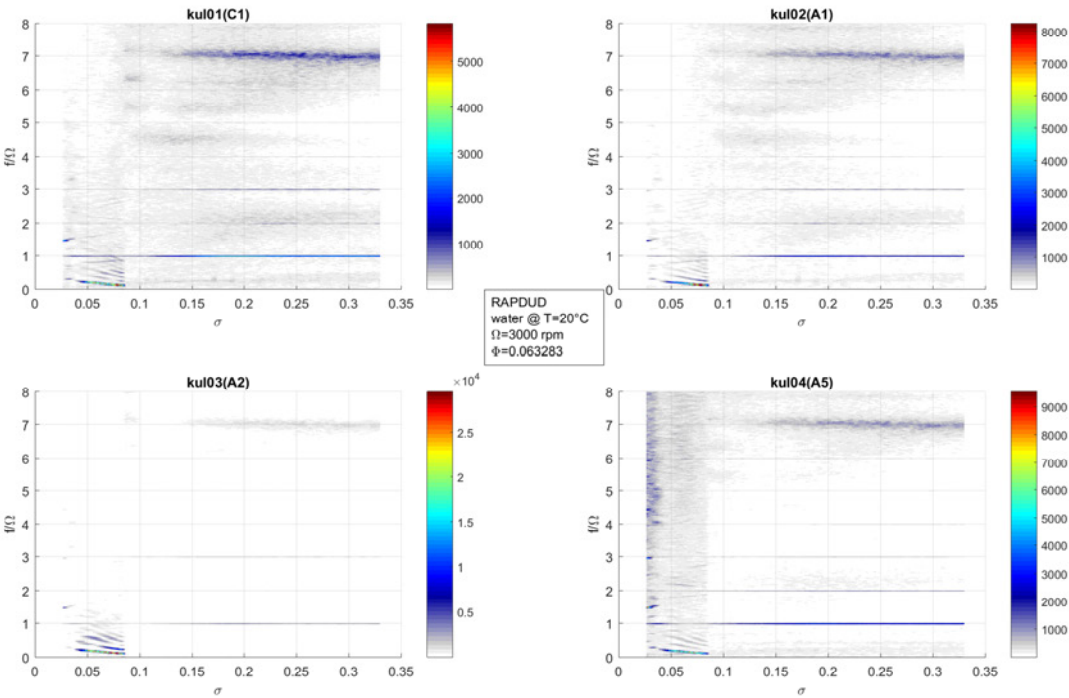


Figure 13. Spectrum of the amplitude of the harmonic pressure oscillations ($|\hat{p}|$) measured by the pressure transducers located in the rotating frame along the blade channels during the test at 90% Φ_D (measured in Pa)

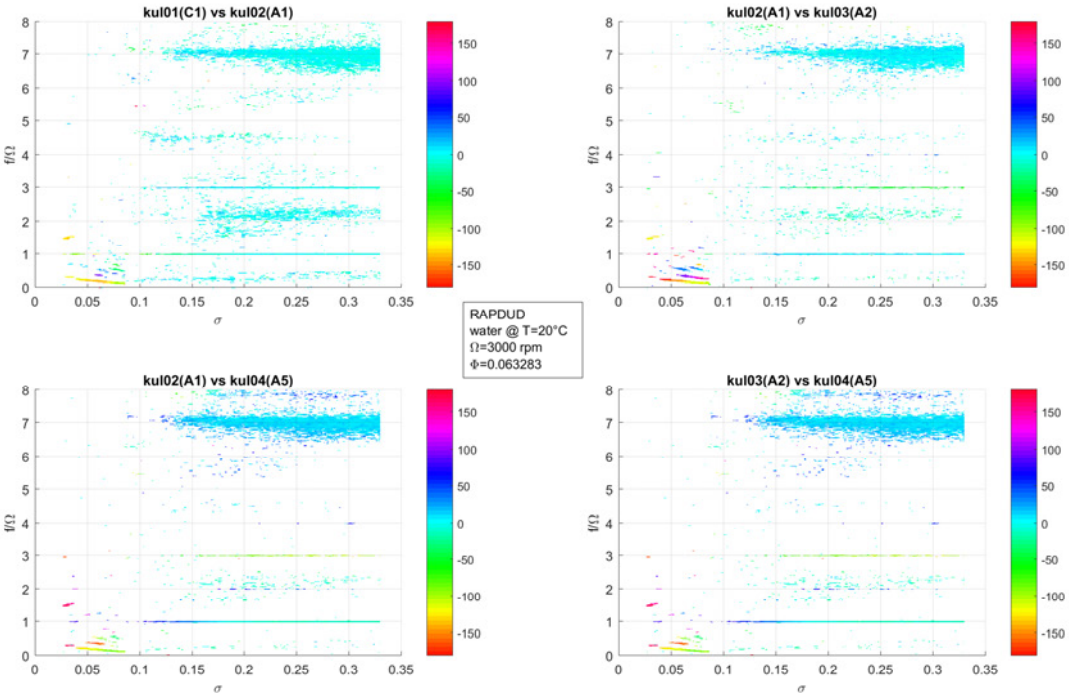


Figure 14. Phases of the cross-spectra of the pressure transducers located in the rotating frame along the blade channels during the test at 90% Φ_D (measured in degrees)

3.3 Estimation of the Flow Oscillations

By means of the characteristic performance surface of the pump experimentally determined (see Figure 6), the gradient of the head coefficient in both the relevant directions (i.e. the cavitation number and the flow coefficient) can be estimated for all the tested flow coefficients at each cavitation number. Moreover, the inertance of the inducer can be estimated from the geometrical features of the inducer by supposing a fully-guided mean flow. Finally, the intensity of the pressure oscillations is determined by the spectral analysis and the phase shift by the phase of the cross-spectrum.

Therefore, the magnitude of the mean flow coefficient oscillations for each experiment at fixed flow rate can be computed as a function of the flow instability frequency and of the cavitation number.

The results are reported from Figure 15 to Figure 18.

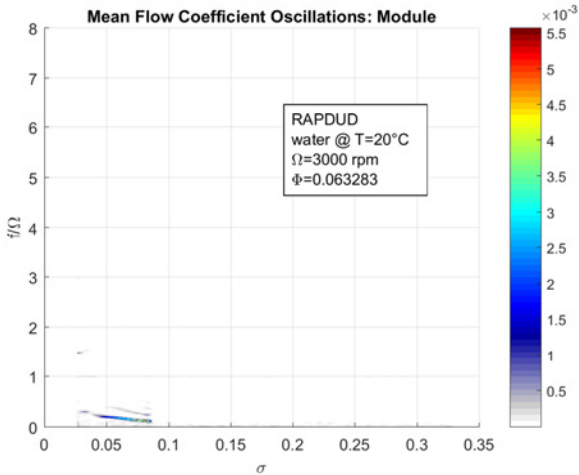


Figure 15. Estimated spectrum of the amplitude of the harmonic oscillations of the mean flow coefficient ($|\hat{\phi}|$) during the test at 90% Φ_D

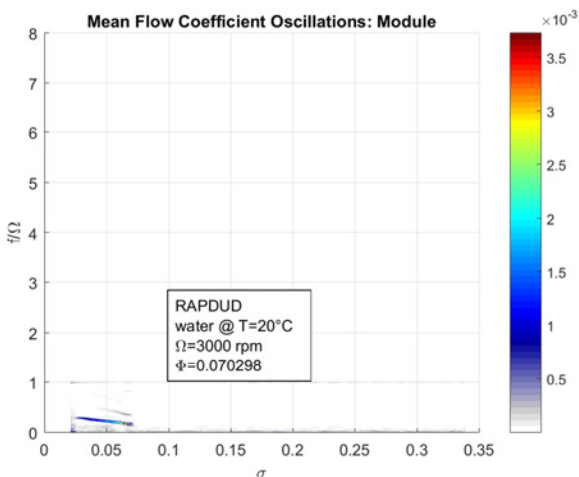


Figure 16. Estimated spectrum of the amplitude of the harmonic oscillations of the mean flow coefficient ($|\hat{\phi}|$) during the test at 100% Φ_D

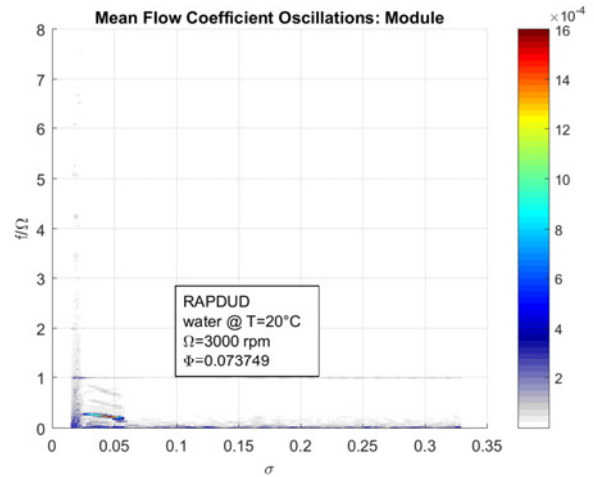


Figure 17. Estimated spectrum of the amplitude of the harmonic oscillations of the mean flow coefficient ($|\hat{\phi}|$) during the test at 105% Φ_D

At 90% Φ_D (see Figure 15), the oscillations associated to the rotating cavitation are particularly intense and result in a significant volumetric flow rate oscillation at the frequency $|\Omega - f_{RC}|$. In terms of dimensionless value, the mean flow coefficient oscillation reaches a peak in the intensity equal to 5.5×10^{-3} that is close to the 9% of the flow coefficient of the experiment. The other relevant instability, such as the high order axial oscillation at roughly 7Ω , does not produce significant mean flow rate oscillations because the pressure oscillations are almost in phase and with the same intensity and the head coefficient is not significantly affected in the relevant range of the cavitation number associated to this type of instability ($\partial \psi / \partial \sigma|_{\phi} \cong 0$).

For the other flow coefficients (see from Figure 16 to Figure 18), as long as the rotating cavitation is present, the corresponding mean flow rate oscillation is estimated. According to the weakening of the rotating instability with the increase of the flow coefficient, the oscillations in the mean flow rate decrease with the increase of the flow coefficient (5% of Φ at 100% Φ_D and 2% of Φ at 105% Φ_D). Consistently with the disappearing of the rotating cavitation at 110% Φ_D , the mean flow rate oscillation is not detected as reported in Figure 18.

The flow coefficient oscillations upstream and downstream of the inducer differ from the mean flow rate oscillation because of the presence of the oscillations of the cavitating volume. Only an experimental set-up capable of measuring at high frequency the oscillations of the volumetric flow rate guarantees the experimental assessment of these oscillations in the upstream and downstream sections.

However, the low frequencies at which the principal instabilities have been detected during the experimental campaign allows the authors to draw some further considerations.

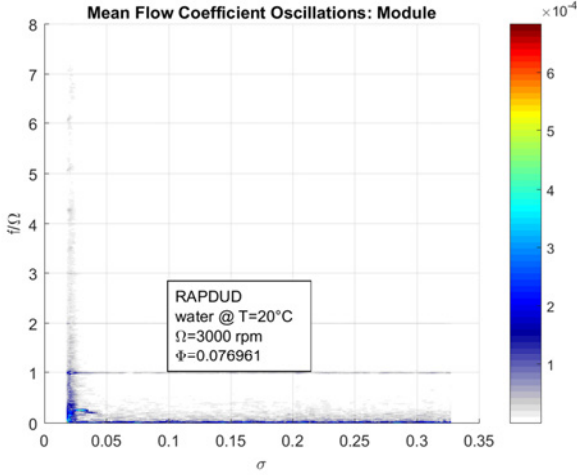


Figure 18. Estimated spectrum of the amplitude of the harmonic oscillations of the mean flow coefficient ($|\hat{\phi}|$) during the test at 110% Φ_D

Due to the triangular inequality, it is possible to estimate an upper and a lower values of the modulus of the oscillations of the flow coefficient in the upstream and downstream sections once the intensity of the mean flow coefficient and the cavitating volume flow coefficient are known:

$$\left| \hat{\phi} - \frac{1}{2} \hat{\phi}_{r_c} \right| \leq \left| \hat{\phi}_{u,d} \right| \leq \left| \hat{\phi} + \frac{1}{2} \hat{\phi}_{r_c} \right| \quad (11)$$

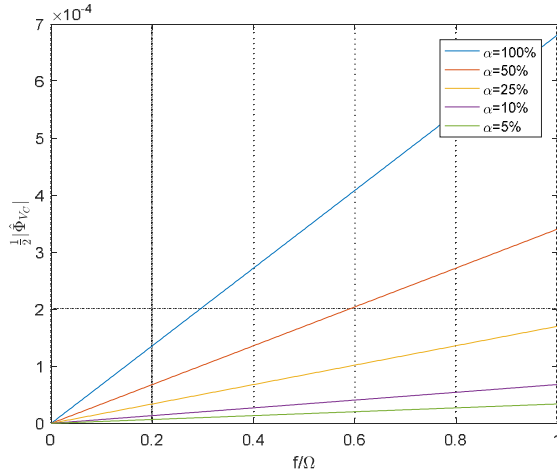


Figure 19. Amplitude of the harmonic oscillations of the flow coefficient associated to the cavitating volume ($|\hat{\phi}_{r_c}|$) at different void fractions as a function of the oscillation frequency

Moreover, the oscillation in the cavitating volume flow coefficient is linear in the frequency of the instability and it is, obviously, limited by the maximum volume available for the cavitating bubble between the two sections selected for the analysis (i.e. the volume available for the working fluid within the channels).

Figure 19 reports the amplitude of the harmonic oscillations of the flow coefficient associated to the cavitating volume for the RAPDUD inducer for different void fraction as a function of the frequency of the instability. For the cavitation surge generated by the

rotating cavitation, the detected frequencies are lower than 0.2Ω and the void fraction is substantially lower than 50%. This implies that the amplitude of the flow rate oscillation associated to the variation of the cavitating volume is significantly lower than 10^{-5} and, consequently, fully negligible with respect to the mean flow rate oscillations computed from the momentum equation. In such condition, the mean flow coefficient oscillation is roughly equal to the upstream and downstream flow coefficient oscillation.

Therefore, the main driver in the generation of the flow coefficient oscillation associated to the rotating cavitation is not the pulsation of the cavitating volume but the redistribution of the pressure experience by each channel during the rotation of the rotating cavitation instability.

4. CONCLUSIONS

The combination of the spectral analysis performed in the stationary and rotating frames proves to be really effective in characterizing the nature and intensity of the cavitation-induced flow instabilities. The rotating cavitation detected in the RAPDUD inducer for a wide range of flow coefficient (from 90% to 105% Φ_D) has been identified in the stationary frame as a sub-synchronous one lobe co-rotating instability and in the rotating frame as a sub-synchronous one lobe counter-rotating instability at a frequency shifted by the rotating speed. The experimental results confirm the weakening of the rotating instability with the increase of the flow coefficient up to the complete disappearance of the rotating cavitation at 110% Φ_D . Moreover, the evaluation of the local cavitation number along the blade channels has highlighted that during this instability the static pressure inside the channel can violently oscillate between the vapor pressure and the collapse peak pressure thus generating significant flow rate oscillations.

The intensity of these flow oscillations, that lead to a cavitation surge, has been estimated for all the relevant flow coefficients through the introduction of a model of the blade channels dynamics that relies on experimental data and on a suitable modelling of the mean flow and cavitating volume oscillations. In particular, the low frequency of this axial instability implies that the oscillation of the cavitating volume can be negligible with respect to the mean flow oscillation generated by the pressure distribution on the boundary of the blade channels due to the rotating cavitation. According to the weakening of the rotating instability with the increase of the flow coefficient, the oscillations in the mean flow rate decrease with the increase of the flow coefficient.

When the onset of the rotating cavitation is unavoidable, the model suggests to increase the inertance of the pump to reduce the intensity of the flow oscillations.

The experimental measurement of the flow oscillations upstream and downstream of the inducer would be beneficial for assessing the soundness of these estimations and is one of the future goals of the authors. Possible experimental set-ups, capable of assessing

these oscillations, would eventually include: electromagnetic flow meters modified for increasing their frequency response, high frequency pressure transducers used to extrapolate the mass flow oscillations inside a duct of known geometry, devices for velocity measurements such as PIV or fiber film probes.

NOMENCLATURE

A	cross-sectional area
c_a	full-bladed axial length
cle	clearance
f	frequency
h_m	mean blade height
L	axial length of the inducer
N_{blade}	number of blades
p	static pressure
p_v	vapor pressure
r_H	inducer hub radius
r_T	inducer tip radius
t	time
T	temperature
V_C	cavitating volume
\dot{V}	volumetric flow rate
x	curvilinear coordinate
α	void fraction
γ	blade angle from axial direction
ρ	density of the working fluid
ρ_L	density of the reference liquid
σ	cavitation number $\sigma = \frac{p_i - p_v}{\frac{1}{2}\rho_L \Omega^2 r_T^2}$
σ_{local}	local cavitation number $\sigma_{local} = \frac{p_{PTj} - p_v}{\frac{1}{2}\rho_L \Omega^2 r_T^2}$
σ_T	tip blade solidity
ϕ	mean flow coefficient $\phi = \frac{(\dot{V}_u + \dot{V}_d)/2}{\pi \Omega r_T^3}$

Φ	local flow coefficient $\Phi_{u,d} = \frac{\dot{V}_{u,d}}{\pi \Omega r_T^3}$
Φ_{V_C}	cavitating volume flow coefficient $\Phi_{V_C} = \frac{\dot{V}_C}{\pi \Omega r_T^3}$
ψ	static head coefficient $\psi = \frac{\Delta p}{\rho_L \Omega^2 r_T^2}$
Ψ	static pressure coefficient $\Psi_{u,d} = \frac{p_{u,d}}{\rho_L \Omega^2 r_T^2}$
Ψ_{ij}	static head coefficient $\Psi_{ij} = \Psi_i - \Psi_j$
ω	pulsation $\omega = 2\pi f$
Ω	inducer rotational speed

Superscripts

\dot{q}	time derivative of q
\bar{q}	quasi-static value of q
\tilde{q}	unsteady value of q
\hat{q}	complex amplitude oscillation of q

Subscripts

1	pump inlet
2	pump outlet
d	downstream
D	design condition
le	blade leading edge
te	blade trailing edge
PTj	pressure tap $j=1, \dots, 5$
u	upstream

Acronyms

Aj	channel A, pressure tap j
AO	Axial Oscillation
Bj	channel B, pressure tap j
Cj	channel C, pressure tap j
$CPRTF$	Cavitating Pump Rotordynamic Test Facility
CS	Cavitation Surge
$kulj$	kulite pressure transducer, name j
$PCBj$	PCB pressure transducer, name j

RC Rotating Cavitation

SFj stationary frame, axial position *j*:

- 1 upstream: 33.3 mm upstream of the tip *le* ;
- 2 mid: 10.7 mm downstream stream of the tip *le* ;
- 3 downstream: 82.7 mm downstream of the tip *le* .

ACKNOWLEDGMENTS

The present work has been possible thanks to the supports of the European Space Agency along several years. The authors would like to express their great gratitude to Dr. Giorgio Saccoccia, ESA-ESTEC, and to Dr. Gianni Pellegrini, Sitael S.p.A.. Special gratitude goes to Lucio Torre that was the pillar of strength of the whole Chemical Propulsion Team for many years.

REFERENCES

- [1] L. Stripling and A. Acosta, "Cavitation in Turbopumps – Part 1," *ASME J. Basic Eng*, vol. 84, pp. 326-338, 01 September 1962.
- [2] L. Sack and H. Nottage, "System Oscillations Associated to Cavitating Inducers," *ASME J. Basic Eng.*, vol. 87, pp. 917-924, 1965.
- [3] M. Natanzon, "Experimental Investigation of Cavitation Induced Oscillations of Helical Inducers," *Fluid Mech. Soviet Res.*, vol. 3, no. 1, pp. 38-45, 1974.
- [4] C. E. Brennen e A. J. Acosta, «Theoretical, Quasi-Static Analysis of Cavitation Compliance in Turbopumps,» *Journal of Spacecraft and Rockets*, vol. 10, n. 3, pp. 175-180, 1973.
- [5] C. E. Brennen e A. J. Acosta, «The Dynamic Transfer Function for a Cavitating Inducer,» *J. Fluids Eng*, vol. 98, n. 2, pp. 182-191, 01 June 1976.
- [6] S. L. Ng and C. E. Brennen, "Experiments on the Dynamic Behavior of Cavitating Pumps," *ASME Journal of Fluids Engineering*, vol. 100, pp. 166-176, 1978.
- [7] D. M. Braisted, "Cavitation induced instabilities associated with turbomachines," California Institute of Technology, Pasadena, California, USA, 1979.
- [8] F. d'Auria, L. d'Agostino e C. E. Brennen, «Bubble Dynamic Effects on the Rotordynamic Forces in Cavitating Inducers,» in *Cavitation and Multiphase Flow Forum. Fluids Engineering Division*, New York, 1995.
- [9] L. d'Agostino, F. d'Auria e C. E. Brennen, «A Three-Dimensional Analysis of Rotordynamic Forces on Whirling and Cavitating Helical Inducers,» *J. Fluids Eng*, vol. 120, n. 4, pp. 698-704, 01 December 1998.
- [10] L. d'Agostino e M. R. Venturini-Autieri, «Rotordynamic Fluid Forces on Whirling and Cavitating Radial Impellers,» in *Fifth International Symposium on Cavitation (cav2003)*, Osaka, Japan, 2003.
- [11] L. d'Agostino e M. R. Venturini-Autieri, «Three-Dimensional Analysis of Rotordynamic Fluid Forces on Whirling and Cavitating Finite-Length Inducers,» in *9th Int. Symp. on Transport Phenomena and Dynamics of Rotating Machinery (ISROMAC-9)*, Honolulu, Hawaii, USA, 2002.
- [12] S. Rubin, "Longitudinal Instability of Liquid Rockets Due to Propulsion Feedback (POGO)," *Journal of Spacecraft and Rockets*, vol. 3, no. 8, pp. 1188-1195, 1966.
- [13] NASA SP-8055, Prevention of Coupled Structure-Propulsion Instability, 1970.
- [14] K. Kamijo, T. Shimura and M. Watanabe, "An Experimental Investigation of Cavitating Inducer Instability," *ASME Paper n. 77-WA/FW-14*, 1977.
- [15] G. Pace, A. Pasini, L. Torre, D. Valentini e L. d'Agostino, «The Cavitating Pump Rotordynamic Test Facility at ALTA S.p.A.: Upgraded Capabilities of a Unique Test Rig,» in *Space Propulsion Conference*, Boredeaux, France, 2012.
- [16] G. Pace, D. Valentini, A. Pasini, R. Hadavandi e L. d'Agostino, «Analysis of Flow Instabilities on a Three-Bladed Axial Inducer in Fixed and Rotating Frame,» in *International Symposium on Transport Phenomena and Dynamic of Rotating Machinery - ISROMAC 2017*, Maui, Hawaii, USA, 2017.
- [17] A. Fujii, Y. Kawamura, T. Hidaka, M. Uchiumi, Y. Yoshida and Y. Tsujimoto, "Higher Order Rotating Cavitation in an Inducer under Head Break Down," in *10th International Symposium on Transport Phenomena and Dynamics of Rotating Machinery (ISROMAC-10)*, Honolulu, Hawaii, USA, 2004.
- [18] L. d'Agostino, L. Torre, A. Pasini and A. Cervone, "A Reduced Order Model for Preliminary Design and Performance Prediction of Tapered Inducer," in *12th International Symposium on Transport Phenomena and Dynamics of Rotating Machinery (ISROMAC-12)*, Honolulu, Hawaii, USA, 2008.
- [19] C. E. Brennen, *Hydrodynamics of Pumps*, New York: Oxford University Press, 1994.
- [20] T. Zoladz, "Observations on Rotating Cavitation and Cavitation Surge from the Development of the Fastrac Engine Turbopump," in *36th AIAA/ASME/SAE/ASEE Joint Propulsion Conference*, Huntsville, AL, USA, 2000.
- [21] L. d'Agostino, L. Torre, A. Pasini e A. Cervone, «On the Preliminary Design and Noncavitating Performance of Tapered Axial Inducers,» *Journal of Fluids Engineering*, vol. 130, n. 11, 2008.